

Dynamical downscaling of future sea level change in the western North Pacific using ROMS

Zhao-Jun Liu^{1,2}  · Shoshiro Minobe¹ · Yoshi N. Sasaki¹ · Mio Terada¹

Received: 28 December 2015 / Revised: 2 July 2016 / Accepted: 4 July 2016 / Published online: 13 July 2016
© The Oceanographic Society of Japan and Springer Japan 2016

Abstract The future regional sea level (RSL) rise in the western North Pacific is investigated by dynamical downscaling with the Regional Ocean Modeling System (ROMS) with an eddy-permitting resolution based on three global climate models—MIROC-ESM, CSIRO-Mk3.6.0, and GFDL-CM3—under the highest greenhouse-gas emission scenario. The historical run is forced by the air-sea fluxes calculated from Coordinated Ocean Reference Experiment version 2 (COREv2) data. Three future runs—ROMS-MIROC, ROMS-CSIRO, and ROMS-GFDL—are forced with an atmospheric field constructed by adding the difference between the climate model parameters for the twenty-first and twentieth century to fields in the historical run. In all downscaling, the RSL rise along the eastern coast of Japan is generally half or less of the RSL rise maxima off the eastern coast. The projected regional (total) sea level rises along the Honshu coast during 2081–2100 relative to 1981–2000 are 19–25 (98–104), 6–15 (71–80), and 8–14 (80–86) cm in ROMS-MIROC, ROMS-CSIRO, and ROMS-GFDL, respectively. The discrepancies of the RSL rise along the Honshu coast between the climate models and downscaling are less than 10 cm. The RSL changes in the Kuroshio Extension (KE) region in all downscaling simulations are related to the changes of KE (northward shift or intensification) with climate change.

Keywords Dynamical downscaling · Regional sea level rise · Western North Pacific · ROMS · CMIP5 climate models · Global warming

1 Introduction

Sea level rise due to global warming is one of the most important changes that the oceans will undergo. Global mean sea level has risen at a rate of 3.2 ± 0.4 mm year⁻¹ in the period 1993–2012 based on satellite altimeter sea surface height (SSH) observations (Cazenave and Cozannet 2013). The recent Intergovernmental Panel on Climate Change (IPCC) Fifth Assessment Report (AR5) indicated that the global mean sea level rise in the 5–95 % possibility range for the period 2081–2100 compared with 1986–2005 is likely to be 45–82 cm for the highest emission scenario Representative Concentration Pathway (RCP) 8.5 (Church et al. 2013).

Observational analysis (Bindoff et al. 2007; Cazenave and Cozannet 2013) and coupled climate models (Landerer et al. 2007; Yin et al. 2010; Yin 2012) indicate that sea level changes in response to a changing climate are not geographically uniform, and show substantial regionality. Based on the satellite records for 1993–2012, the sea level in the western tropical Pacific and eastern Indian Oceans increased much faster than the global mean. In the Atlantic, the sea level rose over the whole basin except for the Gulf Stream region in this period, whereas the sea level fell in the eastern tropical Pacific (Cazenave and Cozannet 2013). Using ensemble projections of 12 models of Coupled Model Intercomparison Project Phase 3 (CMIP3) under the Special Report on Emission Scenario A1B, Yin et al. (2010) calculated the dynamic sea level (sea level deviation from the geoid) during 2091–2100 relative to 1981–2000,

✉ Zhao-Jun Liu
zjliu@mail.sci.hokudai.ac.jp

¹ Department of Natural History Sciences, Graduate School of Science, Hokkaido University, Sapporo, Japan

² State Key Laboratory of Satellite Ocean Environment Dynamics, Second Institute of Oceanography, State Oceanic Administration, 36 Baochubei Road, Hangzhou 310012, China

and found dipole sea level rise patterns in the North Atlantic and North Pacific, and a belt-like pattern in the Southern Ocean. Furthermore, Yin (2012) analyzed 34 models of the Coupled Model Intercomparison Project Phase 5 (CMIP5) and found that there is overall consistency between the projections of regional sea level (RSL, the deviation of SSH from the global mean value) change by the end of the twenty-first century based on the CMIP5 and CMIP3 models for similar scenarios. Major mechanisms for non-uniform dynamical sea level changes are surface wind changes and surface heat and freshwater flux changes. (Sakamoto et al. 2005; Sato et al. 2006; Lowe and Gregory 2006; Landerer et al. 2007; Yin et al. 2010; Suzuki and Ishii 2011a; Sueyoshi and Yasuda 2012; Zhang et al. 2014).

In response to global warming, the future sea level rise in the North Pacific will increase dramatically in the western subtropical gyre east of Japan (Yin et al. 2010; Yin 2012; Sueyoshi and Yasuda 2012). The large sea level rise is related to changes in the Kuroshio Extension (KE), which has a steep meridional sea level gradient, or to larger heat uptake of water masses. Sasaki et al. (2014) recently showed the large sea level variability in the KE region in relation to meridional shifts of the KE jet on decadal time-scales, based on tide-gauge and satellite-derived SSH data. Using an atmosphere–ocean coupled climate model, Sakamoto et al. (2005) showed a large sea level rise south of the KE associated with the intensification of the KE in response to global warming. In contrast, Sato et al. (2006) showed a large sea level rise east of Japan associated with a poleward shift of the KE by using a North Pacific Ocean general circulation model. Sueyoshi and Yasuda (2012) analyzed 15 CMIP3 models and found that some models exhibit a larger northward shift of the KE, and that others exhibit a greater intensification of the KE. They further suggested that different projected changes in the wind stress caused by changes in atmospheric circulations over the North Pacific result in different responses of the KE, which characterize the different patterns of RSL rise in the western North Pacific. Suzuki and Ishii (2011a) investigated sea level changes caused by CO₂-induced climate warming by using an atmosphere–ocean coupled climate model. They found that heat flux changes are more important than wind stress changes for the RSL rise in the southern recirculation of the KE in their model. Suzuki and Ishii (2011b) decomposed baroclinic sea level changes based on the gridded observational data set into vertical modes, and found that the global warming signals are subducted into the ocean interior. This observation might be related to the formation of the North Pacific subtropical mode water around the KE region and the southern recirculation.

Japan is one of countries most likely to be affected by the sea level rise in the western North Pacific caused by global warming (Hanson et al. 2011). The Organization for

Economic Co-operation and Development report (Nicholls et al. 2008) evaluated the risk of coastal cities over the world for future coastal flooding, and the Japanese cities Tokyo, Osaka-Kobe, and Nagoya are the eighth, 13th, and 17th cities measured by assets most exposed to coastal flooding in the 2070s, respectively. Therefore, there is a practical need for projections of RSL change caused by climate change along the Japanese coast.

However, the response of the Japanese coastal sea level to ocean circulation changes caused by global warming has not yet been adequately studied. Current climate models may not represent coastal sea level changes properly in the western North Pacific, because the model resolutions are too coarse to resolve the narrow western boundary currents and the coastal topographies of islands. The most widely used approach to solve this problem is dynamical downscaling, which has recently been applied to projecting the effects of climate change on oceans (Meier 2006; Sato et al. 2006; Ådlandsvik 2008; Sun et al. 2012; Chamberlain et al. 2012; Liu et al. 2013, 2015; Oliver and Holbrook 2014; Seo et al. 2014). For example, Sato et al. (2006) conducted dynamical downscaling to study global warming-induced changes in North Pacific Ocean circulations around Japan by using a North Pacific Ocean general circulation model driven by the sea surface flux derived from MRI-CGCM2.2, which is a climate model contributing to CMIP3. Their model covers the domain 15°S–65°N and 100°E–75°W, with a horizontal resolution of 1/4° (zonally) and 1/6° (meridionally). They reported that coastal sea level rise along Japan is 12–18 cm (including the global mean thermal expansion of 10 cm, but ignoring land-ice melt etc.) from 2000 to 2070, smaller than the 40 cm sea level rise off the east of Japan. However, the spatial distribution of sea level changes along the Japanese coasts was not mentioned by Sato et al. (2006). Moreover, because they did not choose the climate model to be downscaled with a strategy for future sea level rise, it is not clear whether or not their results, obtained from downscaling of only one climate model, are representative. Different climate models produce different sea level changes (e.g., Sueyoshi and Yasuda 2012). Seo et al. (2014) performed dynamical downscaling for the North Pacific marginal seas, and thus their regional model covers the area 118°E–155°E and 18°N–50°N, which may be suitable for these marginal seas, but not for the western North Pacific to the east of Japan. Therefore, downscaling of future RSL changes in the western North Pacific with an appropriate strategy is required. In this study, we examine future Japanese coastal RSL rise by dynamical downscaling with the Regional Ocean Modeling System (ROMS) based on CMIP5 models outputs. For proper representation of western boundary currents, which result from basin-scale atmospheric forcing, the ROMS domain should cover the whole zonal extent of the North

Pacific basin, which is much wider than those in most previous downscaling studies (Meier 2006; Ådlandsvik 2008; Sun et al. 2012; Chamberlain et al. 2012; Liu et al. 2013, 2015; Oliver and Holbrook 2014; Seo et al. 2014). Dynamical downscaling involves a tradeoff between resolution and number of experiments because of the limitation of computational resources. Therefore, we conduct downscaling of three CMIP5 models, which are selected to investigate the worst-case scenario. That is, we choose the three CMIP5 models that are likely to show the largest RSL rise around Japan to evaluate the upper limits of sea level rise.

The rest of the present paper is organized as follows. In Sect. 2, the CMIP5 models used for the downscaling are selected, and the main features of the models are introduced. The methods used to generate the initial conditions, lateral boundary conditions, and the atmospheric forcing fields required for the ROMS are described. In Sect. 3, we compare the downscaled changes and those in the climate model projections and examine the RSL changes around Japan by the end of the twenty-first century. The summary and discussion are presented in Sect. 4.

2 Methods and data

2.1 Global climate models

The CMIP5 climate model simulations used by the IPCC AR5 are mainly accessed through the Program for Climate Model Diagnosis and Intercomparison (PCMDI, website: <http://cmip-pcmdi.llnl.gov/cmip5/>). To project future climate change associated with increasing concentrations of greenhouse gases, the CMIP5 climate models were integrated under some RCP scenarios (Moss et al. 2010). To investigate the possible large sea level rise in the western North Pacific, we focus our attention on the highest emission scenario of RCP8.5 and climate models that have the highest RSL rise near Japan. This strategy will provide the worst-case scenario of RSL rise. Figure 1 shows the spatially averaged projected RSL change over a domain bounded by 25°N–40°N and 125°E–180°E for the 2081–2100 period relative to the 1981–2000 period for 33 CMIP5 models under the RCP8.5 scenario. RSL is evaluated in this study because we are interested in the regional expression of sea level rise. This domain is used for the average because the region shows significant sea level rise in the multi-model ensemble mean from 34 models (Yin 2012). We select the three models with the largest area-averaged RSL rise, which are the MIROC-ESM, the CSIRO-Mk3.6.0, and the GFDL-CM3, as base models for the future dynamical downscaling.

The major features of the three CMIP5 models are as follows. In the MIROC-ESM, the ocean component is

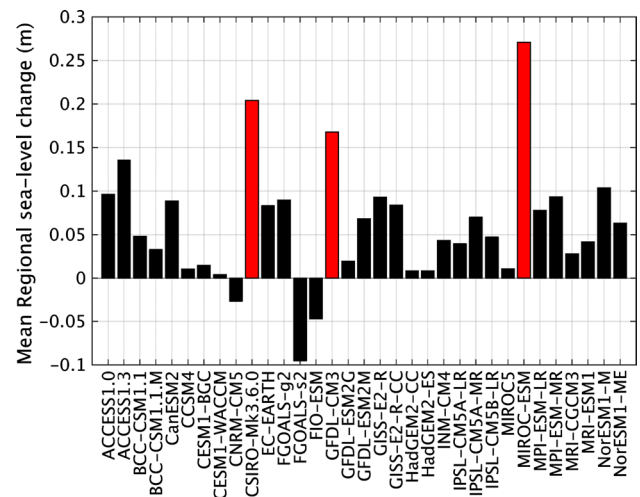


Fig. 1 Projected RSL rises averaged over a domain bounded by 25°–40°N and 125°–180°E during 2081–2100 relative to 1981–2000 for 33 CMIP5 climate models. The three selected models are highlighted in red

the Center for Climate System Research (University of Tokyo) Ocean Component Model (COCO 3.4). The longitudinal grid spacing is about 1.4°, whereas the latitudinal grid intervals gradually vary from 0.5° at the equator to 1.7° near the North/South Poles (Watanabe et al. 2011). In CSIRO-Mk3.6.0, the ocean component is the Modular Ocean Model (MOM 2.2) with a horizontal resolution of 1.875° × 0.9375° (Rotstayn et al. 2010; Jeffrey et al. 2013). The ocean model component of the GFDL-CM3 uses MOM4p1 code. The ocean model resolution is 1° for longitude. The meridional resolution gradually transitions from 1/3° at the equator to 1° at 30°N and remains as 1° between 30°N and 65°N in the Arctic (Griffies et al. 2005, 2011).

2.2 Regional ocean model

The present study uses ROMS to downscale and project sea level changes caused by climate change dynamically. The ROMS can be used for a diverse range of applications from local to planetary scales (e.g., Curchitser et al. 2005; Seo et al. 2007, 2014; Ådlandsvik 2008; Lorenzo et al. 2008; Han et al. 2009). The model solves the incompressible and hydrostatic primitive equations, and uses a free sea surface on horizontally curvilinear coordinates and generalized terrain-following sigma vertical coordinates (Haidvogel et al. 2000; Shchepetkin and McWilliams 2005).

The model domain covers almost the entire North Pacific basin (110°E–100°W, 5°N–50°N) with an eddy-permitting 0.25° × 0.25° horizontal resolution and 32 sigma levels in the vertical direction. The eddy-permitting model has biases, such as the Kuroshio Current overshooting

northward along the eastern coast of Japan (Shu et al. 2013) and the northward shift of the KE (Sumata et al. 2010). Therefore, we examine biases in the model compared with observations, as described in Sect. 3.1, and consider the biases in interpreting the downscaled results.

Schemes used for boundary conditions and mixing are as follows. The radiation lateral boundary condition with nudging (time scale of 30-day) is used for temperature and salinity along the open boundaries at 5°N, 50°N, 110°E, and 100°W that permit long-term stable integration (Seo et al. 2007). A wall boundary condition is chosen for the sea surface elevation and the normal velocity. This is a zero gradient condition for surface elevation and zero flow for the normal velocity (Marchesiello et al. 2001). Harmonic horizontal mixing along an epineutral (constant density) surface is applied to the tracers, whereas biharmonic horizontal mixing along constant sigma surfaces is applied to the momentum. A third-order upstream horizontal advection scheme and fourth-order centered vertical advection scheme for momentum and tracer equations are used (Shchepetkin and McWilliams 2005). K-profile turbulence closure (Large et al. 1994) is used for vertical mixing, and quadratic drag is applied to the bottom friction.

2.3 ROMS experiment settings

(a) Historical run (1951–2000)

The historical run (ROMS-Hist) for the period 1951–2000 provides a reference for interpreting future run results. Initial salinity and potential temperature are set as the climatology of the World Ocean Atlas 2009 (WOA2009) (Locarnini et al. 2010; Antonov et al. 2010), and the initial sea level and velocities are set to zero. At the surface, the historical run is forced with six-hourly winds, air temperature, sea level pressure, specific humidity, daily mean downward shortwave and downward longwave radiation of the Coordinated Ocean Reference Experiment version 2 (COREv2) (Large and Yeager 2009) from 1951 to 2000. The primary data source of COREv2 data set is the NCEP/NCAR R1 reanalysis product; climatological biases in NCEP/NCAR R1 have been corrected in COREv2 on the basis of comparison with more reliable satellite and in situ measurements (Large and Yeager 2009). The effective ocean albedo is set to 0.065 uniformly in the model domain, which is in the appropriate range of this domain. Upward longwave radiation is dependent on simulated sea surface temperature (SST). Surface wind stress and net heat fluxes are computed by using a bulk formula (Fairall et al. 2003). The model sea surface salinity is restored to the climatology values of CORE v2 data with a 30-day period. The lateral boundary values are provided from monthly mean Simple Ocean Data Assimilation version 2.2.4

(SODA 2.2.4) in the period from 1951 to 2000 (Carton and Giese 2008).

(b) Future run (2051–2100)

Because CMIP5 models have biases in parameters that are used for momentum and heat flux calculations in downscaling in the present climate (Lee et al. 2013), the future run in the late twenty-first century is forced with atmospheric fields constructed by adding the monthly mean difference between the CMIP5 model parameters from the twenty-first and twentieth century to the observed parameters, which are mostly six-hourly, in the twentieth century. The details of the approach are as follows. First, we calculate the monthly mean changes between 2051–2100 (RCP8.5) and 1951–2000 (CMIP5 historical) in each month and set of years (e.g., April 2079 minus April 1979) for the simulated winds, air temperature, relative humidity, sea level pressure, net shortwave and downward longwave radiation. Upward longwave radiation is dependent on simulated SST. Secondly, these monthly mean changes are added to CORE v2 atmospheric surface fields for the corresponding month and year for the 1951–2000 period used for ROMS-Hist. Finally, the bulk formula is used to calculate the projected surface fluxes of momentum, and sensible and latent heat, with the parameters determined in the second step. Similarly, the model sea surface salinity at each grid point is restored to the value that is given by the climatology used for historical run added 50-year time series of monthly sea surface salinity differences between the 2051–2100 period and the 1951–2000 period. We also apply this approach to the initial and lateral boundary conditions. The initial conditions for the future runs are also generated by adding the changes in temperature and salinity between January 1951 and January 2051 in the CMIP5 models to the initial condition of ROMS-Hist. The initial sea level and velocities are set to zero in all future runs. The lateral boundary conditions for the future runs are created by adding changes in monthly mean temperature, salinity, and velocity between 2051–2100 and 1951–2000 in the CMIP5 models to the respective fields in SODA 2.2.4 in the period 1951–2000. We call the three ROMS future runs forced by the MIROC-ESM, CSIRO-Mk3.6.0, and GFDL-CM3 variables ROMS-MIROC, ROMS-CSIRO, and ROMS-GFDL, respectively. The last 20 years of the historical run and of all future runs are used in the following analyses.

2.4 Regional sea level

To focus on the regional distribution, we analyze RSL, which is the sea level at each grid point minus the global

mean (e.g., Yin et al. 2010; Zhang et al. 2014). The RSL in the CMIP5 models is given by

$$h'_{CM}(x, y, t) = h_{CM}(x, y, t) - \bar{h}_{CM}^G(t), \quad (1)$$

where h_{CM} is the sea level in a climate model (zos in CMIP5), \bar{h}_{CM}^G is the global mean sea level, t is time, and x and y are the zonal and meridional coordinates, respectively. Because the ROMS domain does not cover the global, the RSL in ROMS simulations is defined by

$$h'_{ROMS}(x, y, t) = h_{ROMS}(x, y, t) - \bar{h}_{CM}^G(t) - (\bar{h}_{ROMS}^G(t) - \bar{h}_{CM}^D(t)), \quad (2)$$

where the h_{ROMS} is the sea level output of ROMS, \bar{h}_{CM}^G is the corresponding CMIP5 model's global mean, \bar{h}_{ROMS}^D and \bar{h}_{CM}^D are the means over the current model domain (110°E–100°W, 5°N–50°N) in ROMS and the CMIP5 models, respectively.

2.5 Observational data

The ROMS-Hist is compared with the following observational data. The maps of weekly absolute dynamic height are compiled from the TOPEX/Poseidon, ERS-1/2, Jason-1,

and Envisat altimeter observations on a $1/3^\circ \times 1/3^\circ$ Mercator spatial resolution grid from January 1993 to December 2000, distributed by the Archiving, Validation and Interpretation of Satellite Oceanographic Data (AVISO) (Ducet et al. 2000). The absolute dynamic height products are computed with consistent sea level anomaly and mean dynamic topography field (Rio and Hernandez 2004).

3 Results

3.1 Comparison of ROMS-Hist and observations

To evaluate the capability of the ROMS downscaling, the time-mean surface velocity obtained from the three CMIP5 models, ROMS-Hist, and satellite data are compared in Fig. 2. Generally, all three CMIP5 models show a broad, weak Kuroshio Current and KE. It should be noted that ROMS-Hist fails to produce some observed features, as expected for an eddy-permitting model (e.g., Kagimoto and Yamagata 1997; Sumata et al. 2010; Shu et al. 2013). The KE is mainly formed roughly along 37°N with a minor eastward flow around 30°N. In the satellite observations, the

Fig. 2 Time-mean surface velocities (colors) and vector velocities (vectors) for 1993–2000 in the three selected CMIP5 climate models (a–c), the ROMS historical run (d), and the satellite-derived surface geostrophic currents (e) (color figure online)

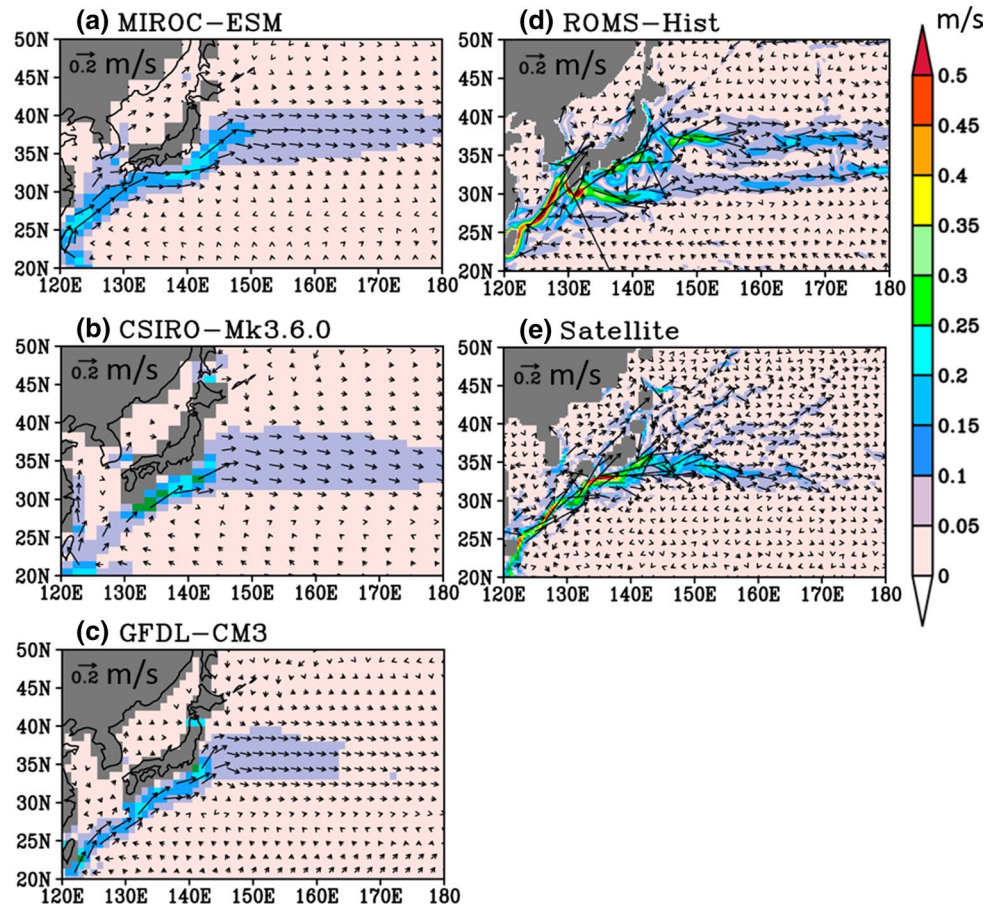
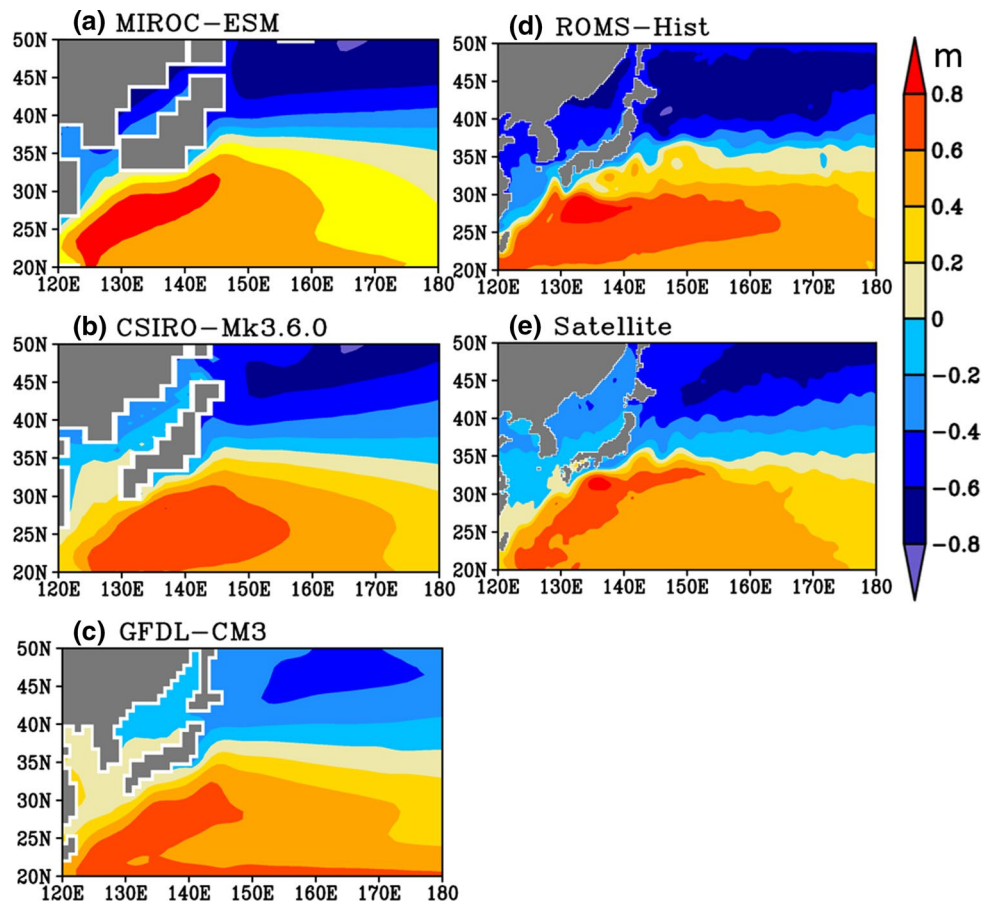


Fig. 3 Time-mean RSL for 1993–2000 period in three CMIP5 climate models (a–c), the ROMS historical run (d), and the satellite observations (e)



Kuroshio Current separates from the coast and turns into the KE around 35°N. The modeled extension around 30°N is associated with the separation of the Kuroshio Current from the coast to the east of Kyushu. The systematic discrepancies between the ROMS-Hist and the observations should be considered in interpreting downscaled future changes.

The different surface current structures among the CMIP5 climate models, ROMS-Hist, and observation are reflected in differences in SSH, because the SSH gradient is closely related to the surface current speeds through the geostrophy. Figure 3 shows that ROMS-Hist exhibits sharp SSH gradients across the Kuroshio Current and the KE as observed, although the CMIP5 climate models have broad, weak gradients especially over the KE. Proper reproduction of sharp SSH gradients is important in sea level changes, because shifts in SSH fronts can produce large sea level changes.

Another deficiency in the CMIP5 climate models is that the three straits connecting the Japan Sea either to the North Pacific Ocean or to marginal seas, such as the Tsushima, Tsugaru, and Soya Straits (Fig. 4), are not properly resolved. The Tsugaru Strait is closed in MIROC-ESM and CSIRO-Mk3.6.0, whereas the Soya Strait is closed in GFDL-CM3. Therefore, examination of future flow changes through the straits is impossible

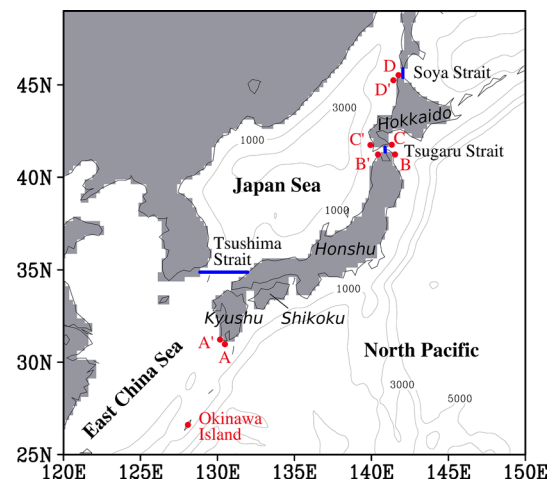
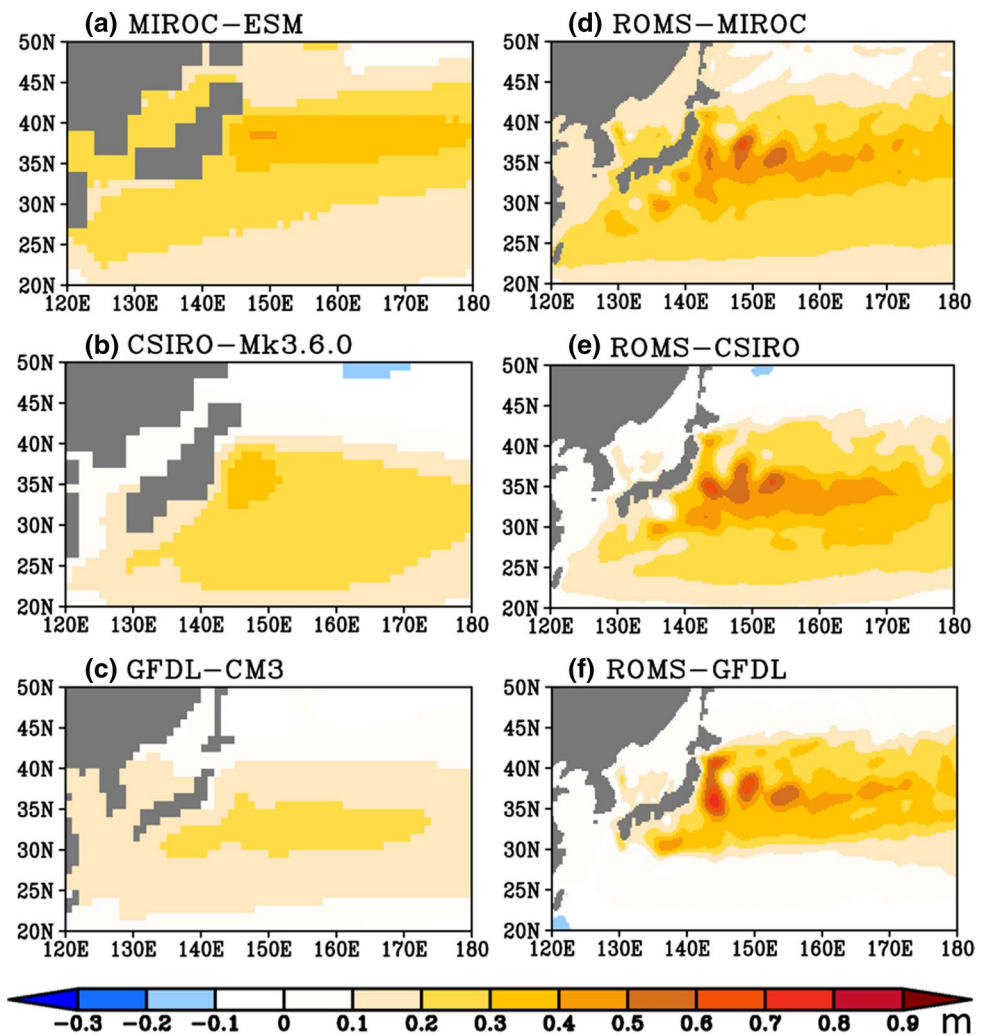


Fig. 4 Topography around Japan from ROMS. *Contours* indicate bathymetric depths in meters, and *gray areas* indicate the land mask. *Blue lines* denote the locations of the Tsushima, Tsugaru, and Soya Straits. *Red dots* denote the coastal stations used in Fig. 9 and the Okinawa Island station (26.75°N, 128°E) in Fig. 10 (color figure online)

using these climate models, but is possible using ROMS downscaling. The observed volume transports are 2.6 Sv ($1 \text{ Sv} = 10^6 \text{ m}^3 \text{ s}^{-1}$) (Fukudome et al. 2010), 1.6 Sv (Ito

Fig. 5 Projected changes in mean RSL around Japan for 2081–2100 relative to 1981–2000 in (left) CMIP5 climate models under the RCP8.5 scenario and in (right) ROMS downscaling simulations. Top, middle, and bottom panels are for MIROC-ESM, CSIRO-Mk3.6.0, and GFDL-CM3, respectively



et al. 2003), and 0.7 Sv (Fukamachi et al. 2010) through the Tsushima, Tsugaru, and Soya Straits, respectively, whereas they are 2.6, 2.4, and 0.2 Sv in ROMS-Hist (Fig. 15). Hence, ROMS-Hist represents the Tsushima Strait throughflow very well, whereas overestimates the Tsugaru Strait and underestimates the Soya Strait throughflow.

3.2 Regional sea level changes around Japan

In this section, we investigate how large the RSL changes around Japan are by the end of twenty-first century under the RCP8.5 scenario. Figure 5 shows the projected changes in mean RSL around Japan during 2081–2100 relative to 1981–2100 in the three CMIP5 models and in the corresponding ROMS downscaling simulations. The three CMIP5 models project RSL rises in the subtropical gyre east of Japan, with a maximal RSL rise of 44, 37, and 27 cm in MIROC-ESM, CSIRO-Mk3.6.0, and GFDL-CM3, respectively.

The RSL changes in the ROMS simulations have finer structures and higher magnitudes than those in the CMIP5 models, with some similarities among different downscaling simulations (Fig. 5). The ROMS downscaling exhibits larger RSL rise maxima than the CMIP5 models; the RSL rise maxima reach 63, 67, and 76 cm in ROMS-MIROC, ROMS-CSIRO, and ROMS-GFDL, respectively. The downscaled RSLs commonly exhibit zonally aligned three maxima along 37°N between 140°E and 160°E. A comparison of these RSL rise patterns with the surface currents at the end of the twenty-first century (Fig. 6) and the end of the twentieth century (Fig. 2) reveals that the RSL rise along 37°N is associated with the northward shift of the KE in ROMS-MIROC and ROMS-GFDL. The relatively large RSL rise at 30°N and 40°N is related to the substantial weakening of the eastward current along 30°N found in ROMS-Hist and to the increased eastward currents around 40°N. It should be noted that in all ROMS simulations, RSL increases larger than 30 cm are limited to seaward of the continental shelf off the Japanese archipelago, so that

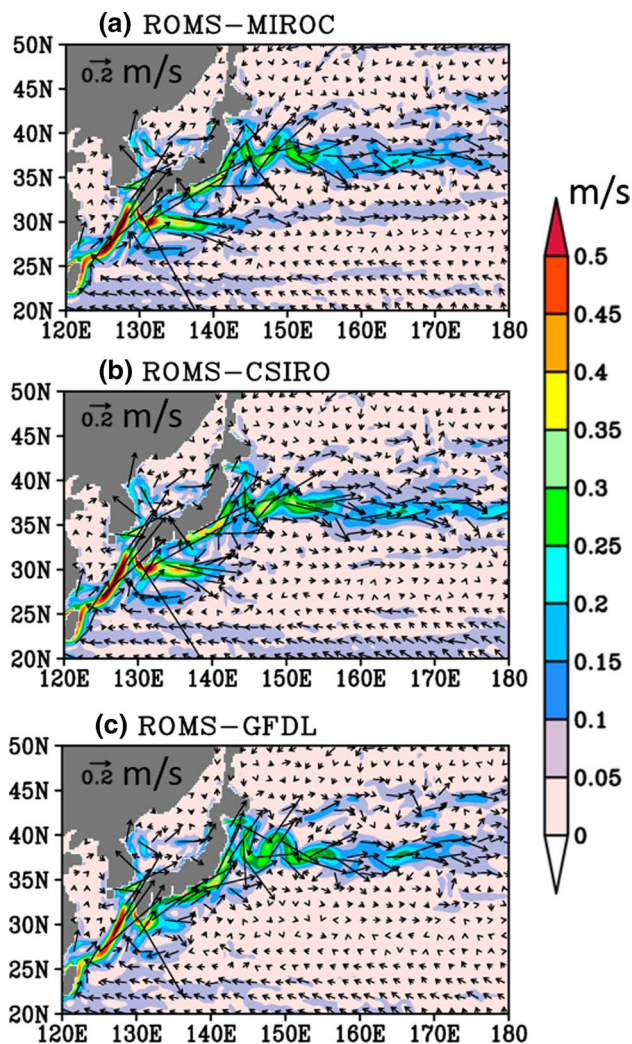


Fig. 6 Time-mean surface absolute velocities (*colors*) and vector velocities (*vectors*) averaged over 2081–2100 in **a** ROMS-MIROC, **b** ROMS-CSIRO, and **c** ROMS-GFDL (color figure online)

the high offshore RSL rise would not reach the coast of Japan.

To better understand the relationship between the offshore and coastal RSL changes, we examine the meridional distribution of the RSL rise zonally averaged over 145°E–155°E and that on the Japanese eastern coast simulated by the CMIP5 models (Fig. 7) and the ROMS downscaling (Fig. 8). We select the coastal RSL as the RSL at the ocean grid located next to the easternmost land grid of Japan at each latitude. In all CMIP5 models and ROMS simulations, the RSL changes along the eastern coast of Japan are generally half or less of the RSL rise maxima off the eastern coast of Japan.

Figure 9 shows RSL rises at all coastal grid points along Honshu Island, which is artificially connected to Kyushu and Shikoku islands forming one island in the ROMS

simulations (Fig. 4), and Hokkaido Island. The coastal RSL changes during 2081–2100 relative to 1981–2000 derived directly from the three CMIP5 models and those obtained from ROMS downscaling are shown in Fig. 9a, b for the eastern and western coasts, respectively. The projected RSL rises during 2081–2100 relative to 1981–2000 along Honshu are 19–25, 6–15, and 8–14 cm in ROMS-MIROC, ROMS-CSIRO, and ROMS-GFDL, respectively. An important feature is that the differences in RSL changes between downscaling simulations and the corresponding CMIP5 models are less than 10 cm along Honshu coast. This means that if a 10 cm discrepancy is allowed at the maximum, we can use climate model outputs directly to assess the RSL rise along Honshu coast. The smaller differences in coastal RSL than in offshore RSL between the ROMS downscaling and climate models are probably caused by coastally trapped shelf waves. These waves tend to average sea level along the coast, resulting in roughly constant coastal sea level, which is given by the average of sea level at the northern and southern ends of the island (Liu and Wu 1999). Tsujino et al. (2008) successfully obtained semi-analytical solution of coastal sea level around Japan arising through adjustment of coastal trapped waves and Rossby waves consistent with their OGCM of similar grid-spacing from the present model. We compared the simulated coastal sea levels and observed sea level anomalies averaged over four stations, which were selected by Japan Meteorological Agency for the most reliable long-available stations, along the Japanese coast in the period of 1971–2000 ($r = 0.37$, significant at the 95 % confidence level). Therefore, the year-to-year variability of the model coastal sea level is consistent with that in the observed sea levels along the Japanese coast. The northward decrease in RSL changes on the western Honshu coast may be consistent with the northward propagation of shelf waves with damping along the route.

Although the RSL rises in the CMIP5 models and in ROMS downscaling are generally similar along Honshu, they can be substantially different at the islands separated from Honshu, because sea levels at those islands are not affected by the averaging effects of coastal waves. Here, we examine sea level change at Okinawa Island (Fig. 4), because extremely high sea levels have occurred there (Tokeshi and Yanagi 2003), suggesting that it is important to project the RSL rise at Okinawa Island in the future warming climate. Although Okinawa Island is too small to be represented as an island in the current ROMS downscaling simulations, sea level changes at the island would be well approximated by the modeled sea level changes at that location. Figure 10 shows the projected RSL changes at Okinawa Island during 2081–2100 relative to 1981–2000 in the three CMIP5 models and corresponding ROMS simulations. Both ROMS-MIROC and ROMS-CSIRO

Fig. 7 (Top) RSL zonally averaged from 145°E to 155°E and temporally averaged for 1981–2000 (blue) and 2081–2100 (red), and (bottom) projected RSL rise zonally averaged from 145° to 155°E (black) and projected Japanese eastern coastal RSL rise (purple) for 2081–2100 relative to 1981–2000 in (left) MIROC-ESM, (middle) CSIRO-Mk3.6.0, and (right) GFDL-CM3 (color figure online)

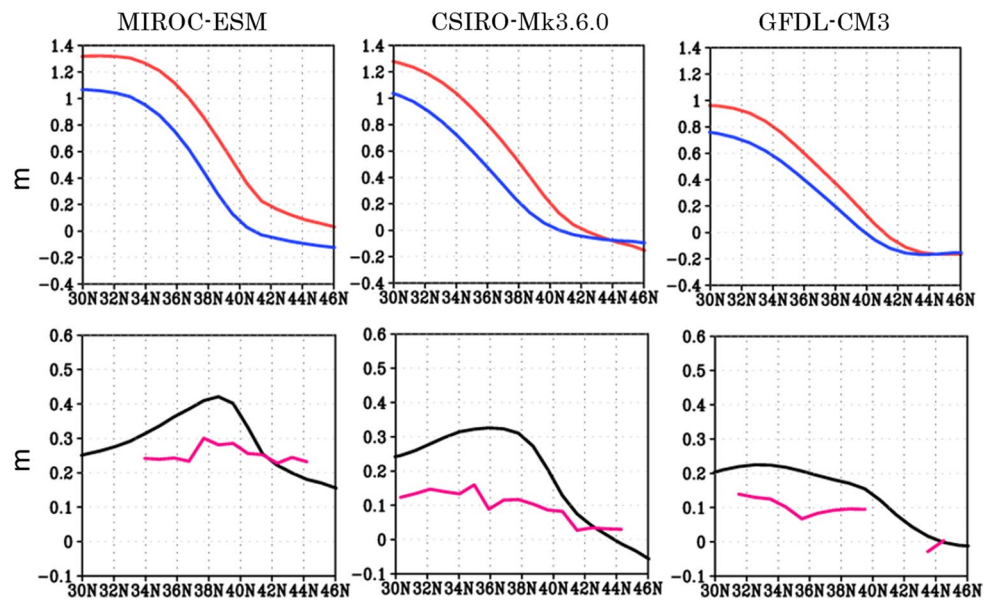
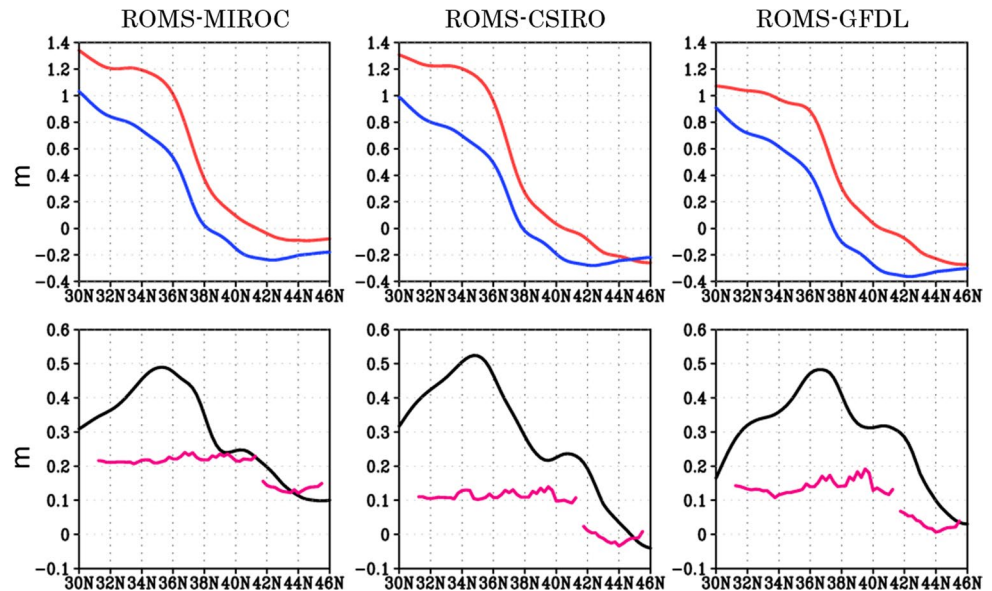


Fig. 8 (Top) RSL zonally averaged from 145°E to 155°E and temporally averaged for 1981–2000 (blue) and 2081–2100 (red), and (bottom) projected RSL rise zonally averaged from 145° to 155°E (black) and projected Japanese eastern coastal RSL rise (purple) for 2081–2100 relative to 1981–2000 for the ROMS downscaling simulations with (left) ROMS-MIROC, (middle) ROMS-CSIRO, and (right) ROMS-GFDL (color figure online)



project high RSL rises at Okinawa Island of 29 and 32 cm, respectively, which are as much as or larger than the RSL rise maxima on the Honshu coast. However, ROMS-GFDL projects relatively small RSL rise at Okinawa Island of 9 cm. The difference between CSIRO-Mk3.6.0 and ROMS-CSIRO is 16 cm, exceeding the aforementioned maximal discrepancy of 10 cm along Honshu coast between the CMIP5 climate model and ROMS downscaling.

3.3 Three-dimensional oceanic changes

As revealed by previous studies, the spatial distributions of RSL rise in the western North Pacific are related to the

upper ocean changes (Sakamoto et al. 2005; Sato et al. 2006; Suzuki and Ishii 2011a; Sueyoshi and Yasuda 2012). In this section, we investigate future changes below the surface in the western North Pacific to understand the relationships between these changes and the RSL rise around Japan.

Sea level changes accompanied by density changes are represented by dynamic height (DH). DH is a commonly used parameter that can be calculated in terms of temperature and salinity by Eq. 3 (Gill 1982) with reference to 2000 dbar.

$$\Delta DH = \frac{1}{g} \int_{2000}^0 (v_s(S, T, p) - v_s(35\text{psu}, 0^\circ\text{C}, p)) dp, \quad (3)$$

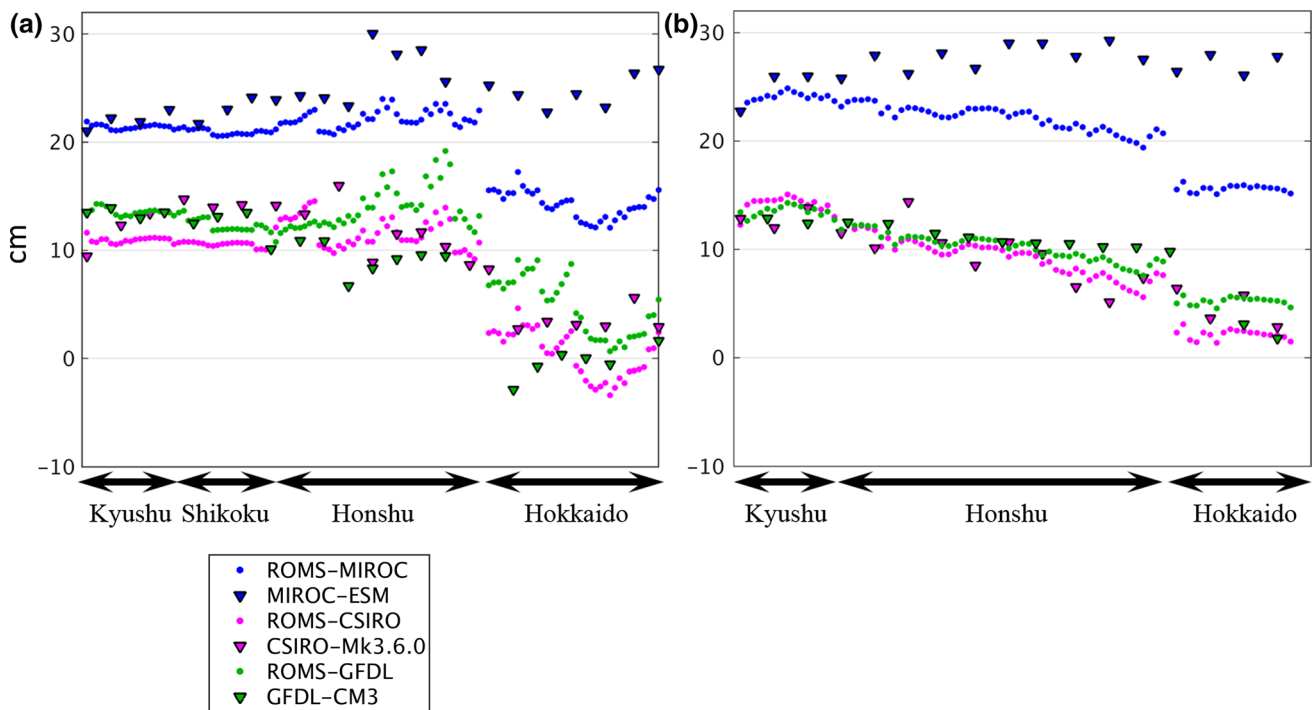


Fig. 9 Projected Japanese eastern (a) and western (b) coastal RSL rise for 2081–2100 relative to 1981–2000 in three CMIP5 models (triangles) and from ROMS simulations (dots), with MIROC-ESM

and ROMS-MIROC (blue), CSIRO-Mk3.6.0 and ROMS-CSIRO (purple), and GFDL-CM3 and ROMS-GFDL (green) (color figure online)

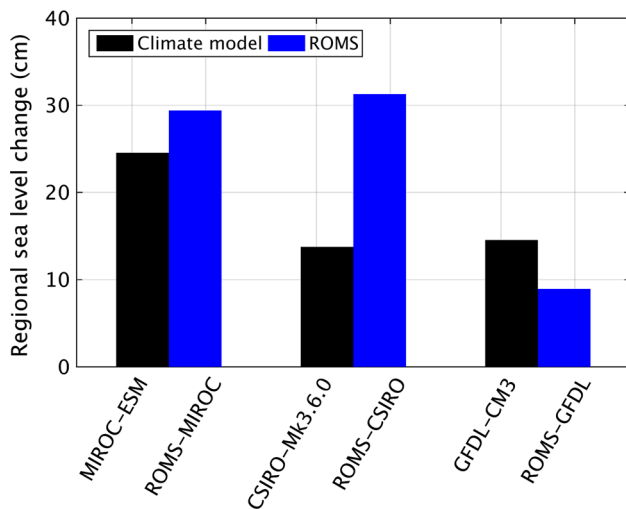


Fig. 10 Projected RSL rise (in centimeters) at Okinawa Island (26.75°N, 128°E, as shown in Fig. 4) during 2081–2100 relative to 1981–2000 in MIROC-ESM, CSIRO-Mk3.6.0, and GFDL-CM3 (black bars), and in the corresponding ROMS downscaling simulations (blue bars) (color figure online)

here, S is salinity, T is temperature, g is acceleration due to gravity, and v_s is specific volume, given by the reciprocal of in situ density, and the anomaly of specific volume is defined as the specific volume related to that at the same

pressure for salinity of 35 psu and temperature of 0 °C. Thus, DH is defined as the vertical integration of the specific volume anomaly from the pressure of 2000–0 dbar (at the surface). For consistency with the RSL rise, regional dynamic height (RDH) is defined in a similar manner to the RSL definition (Eq. 2) as

$$\Delta DH'_{ROMS} = \Delta DH_{ROMS} - \overline{\Delta DH}_{CM}^G - (\overline{\Delta DH}_{ROMS}^D - \overline{DH}_{CM}^D), \quad (4)$$

where the ΔDH_{ROMS} is DH calculated by the ROMS outputs, $\overline{\Delta DH}_{CM}^G$ is the corresponding CMIP5 model's global mean DH, $\overline{\Delta DH}_{ROMS}^D$ and $\overline{\Delta DH}_{CM}^D$ are the DH means over the North Pacific ROMS domain in ROMS and the CMIP5 models, respectively.

Figure 11 shows the RDH changes during 2081–2100 relative to 1981–2000 obtained from the three ROMS downscaling simulations. The comparison of the RDH changes (Fig. 11a–c) and RSL rises (Fig. 5d–f) indicate that the RDH changes very well reproduce the major features of RSL rises described in the previous section, including RSL rises associated with the KE changes.

We examine subsurface signatures related to RSL rises that penetrate downward. Figure 12 shows projected changes in mean eastward velocity zonally averaged from 145°E to 155°E in a meridional-vertical cross section across the KE during 2081–2100 relative to 1981–2000

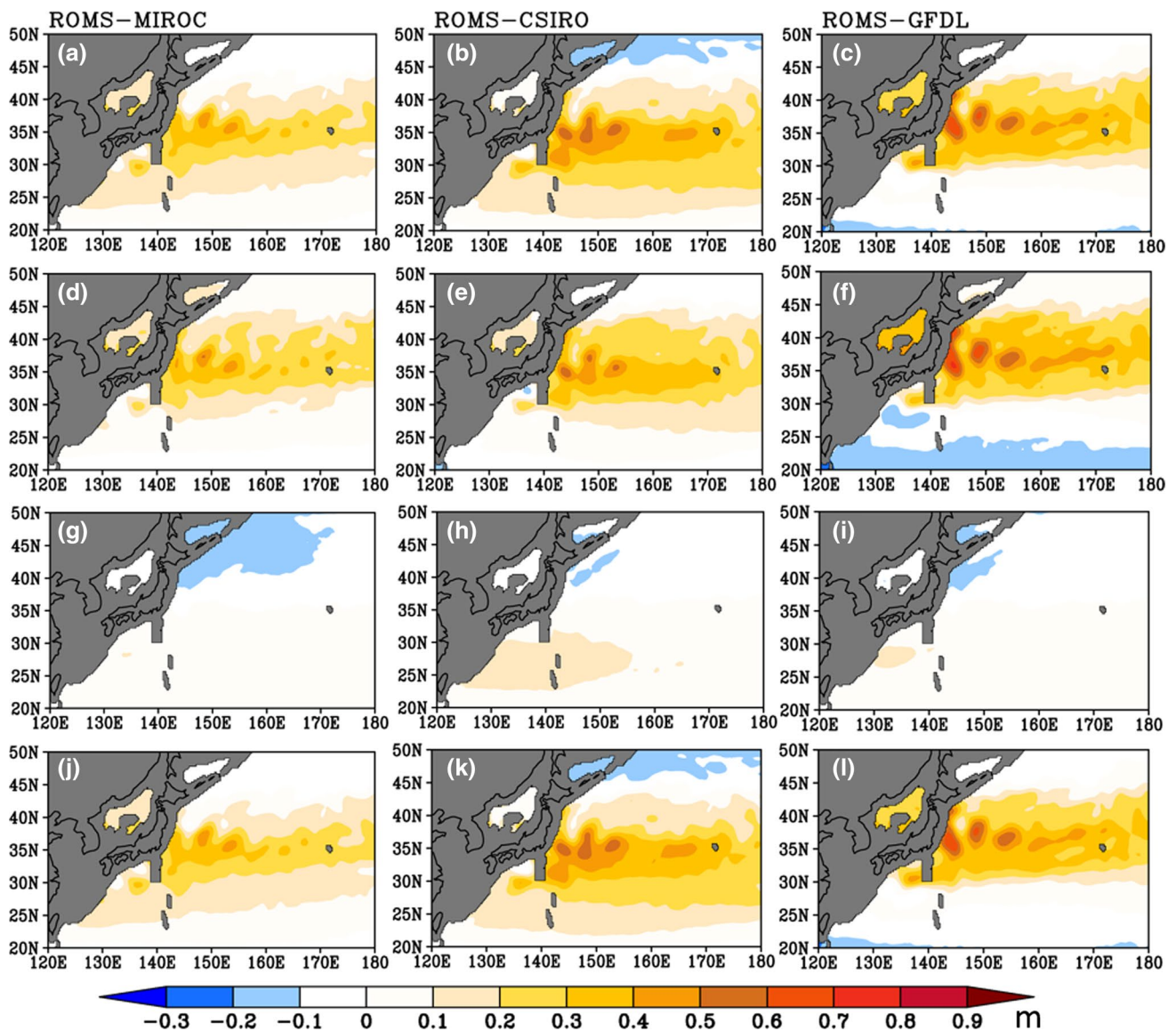


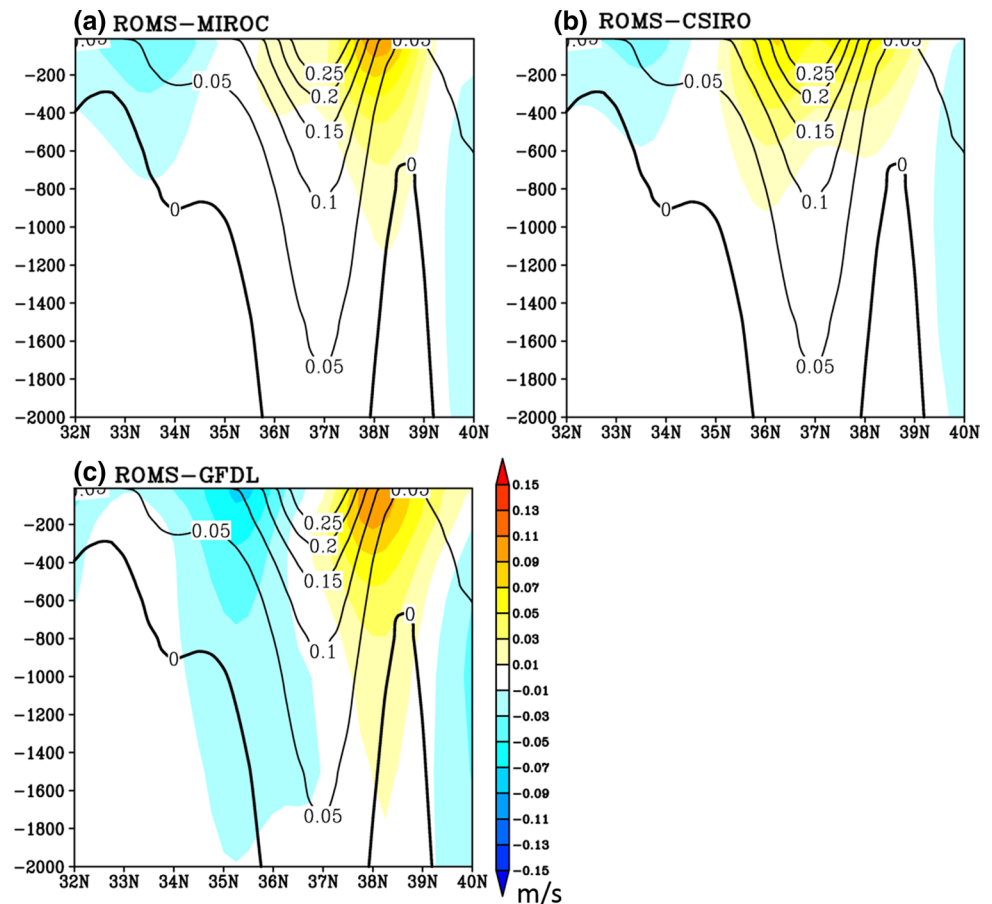
Fig. 11 a–c RDH changes with reference to 2000 dbar during 2081–2100 relative to the 1981–2000 period, d–f RDH changes due to the thermosteric component, and g–i RDH changes due to halos-

teric components, and j–l the sum of the thermosteric and halosteric components, in (left) ROMS-MIROC, (middle) ROMS-CSIRO, and (right) ROMS-GFDL

in the ROMS simulations. The zonal velocity changes are consistent with the aforementioned KE changes. Velocity increase in ROMS-CSIRO is collocated with the KE in the twentieth century, indicating the KE intensification. In ROMS-GFDL, velocity increases (decreases) to the north (south) of the KE axis in the twentieth century, showing the northward migration of the KE axis. In ROMS-MIROC, strong velocity increase is found to the north of the twentieth century KE axis but weak increase occurs almost over the whole KE axis, suggestive of the combination of the northward migration and overall intensification. The zonal velocity changes mainly occur in the upper 1000 m, and penetrate down to 2000 m in ROMS-GFDL. The vertical

penetration may suggest that this pattern is unlikely to be caused by heat or fresh water fluxes at the surface. This is because such thermohaline flux changes would cause temperature and salinity changes primarily limited to major water masses such as subtropical mode water at depths of 300–400 m or shallower (Suzuki and Ishii 2011b). Therefore, these changes are probably forced by wind stress changes (e.g., Sakamoto et al. 2005; Sato et al. 2006; Sueyoshi and Yasuda 2012). The velocity changes in ROMS-MIROC and ROMS-CSIRO penetrate to a shallower depth than ROMS-GFDL. In addition, in ROMS-CSIRO, near surface decrease of density is much more prominent than in the other two models (not shown). These features in

Fig. 12 Projected changes in mean eastward velocity zonally averaged from 145°E to 155°E for 2081–2100 relative to 1981–2000 (colors) in **a** ROMS-MIROC, **b** ROMS-CSIRO, and **c** ROMS-GFDL. Contours show the mean distribution for 1981–2000. The contour interval is 0.05 m/s (color figure online)



ROMS-CSIRO suggest that water mass changes may play a more important role in the RSL in this model than in the others, while both the effects of wind stress changes and water mass changes are all included in ROMS-MIROC. Temperature changes penetrate to 2000 m, which is consistent with the zonal velocity changes of the KE (Fig. 13), whereas the vertical penetration of the salinity changes are limited to the upper 1000 m, because of the lack of mean salinity gradients deeper than 1000 m (not shown). All ROMS simulations commonly show that the positive Sverdrup function changes east of Japan (Fig. 14) are caused by the negative wind stress curl changes over the North Pacific (not shown).

The RDH changes shown in Fig. 11a–c are decomposed into thermosteric and halosteric components. The decomposition methods are described in Eqs. (5) and (6) (Landerer et al. 2007; Zhang et al. 2014).

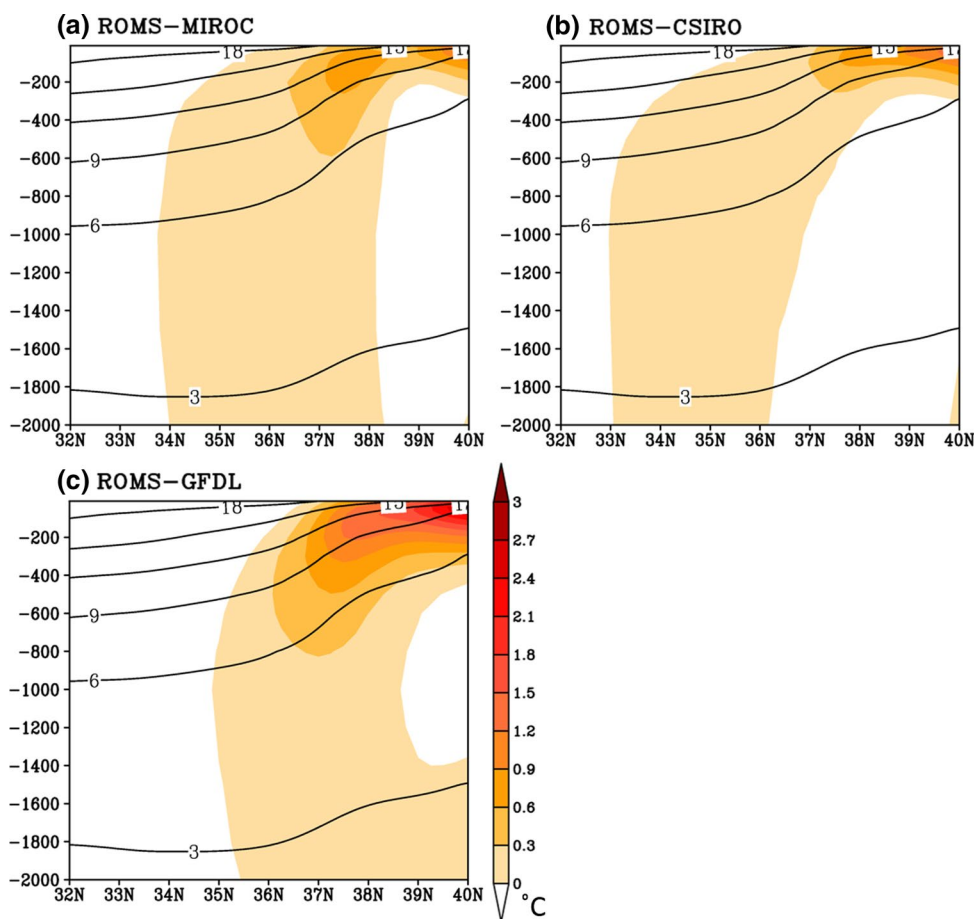
$$\Delta DH_T = \frac{1}{g} \int_{2000}^0 (v_s(35 \text{ psu}, T, p) - v_s(35 \text{ psu}, 0^\circ \text{C}, p)) dp \quad (5)$$

$$\Delta DH_S = \frac{1}{g} \int_{2000}^0 (v_s(S, 0^\circ \text{C}, p) - v_s(35 \text{ psu}, 0^\circ \text{C}, p)) dp \quad (6)$$

Here, ΔDH_T and ΔDH_S are the thermosteric and halosteric DH, respectively. The calculation of regional thermosteric and halosteric DH is similar to that of RDH given in Eq. (4). Figure 11d–f and g–i show the regional thermosteric and halosteric contributions, respectively, to RDH changes during 2081–2100 relative to 1981–2000. The sum of these two components recovers the RDH changes well (Fig. 11j–l). Thus, although the density is a nonlinear function of temperature, salinity and depth, its nonlinearity is weak with respect to temperature and salinity differences caused by the climate change. In all ROMS simulations, thermosteric components dominate the RDH change between 30°N and 40°N. Smaller halosteric components contribute to producing a larger RDH to the south than to the north. Consequently, the thermosteric component gives the major RDH, and thus the major RSL rise features, whereas the effect of halosteric component is small.

The spatial structure of the sea level changes may be associated with changes in the throughflow transport via the Tsugaru, Tsushima, and Soya Straits, because differences in sea level between the upstream and downstream of a strait strongly constrain throughflows (Ohshima 1994; Lyu and Kim 2005; Tsujino et al. 2008). Figure 15 shows the time-mean volume transports during 1981–2000 period and

Fig. 13 Projected changes in potential temperature (in °C, color shading, meridional average has been removed at each depth) zonally averaged from 145°E to 155°E for 2081–2100 relative to 1981–2000 in **a** ROMS-MIROC, **b** ROMS-CSIRO, and **c** ROMS-GFDL along with their mean value for 1981–2000 (*contours*). The contour interval is 3 °C



2081–2100 period through the Tsushima, Tsugaru, and Soya Straits in ROMS downscaling. All transports through the straits will increase in the future warming climate. ROMS-CSIRO projects a much larger increase in the transports of each strait compared with the other two downscaling simulations. This is probably because ROMS-CSIRO projects a negative RSL rise in the subpolar gyre (Fig. 5), in contrast to the positive RSL rise in the other two models. The negative RSL rise in the subpolar gyre, combined with the positive RSL rise in the subtropical gyre is associated with the larger increase in SSH difference between the subpolar and subtropical gyres in ROMS-CSIRO than in other two models.

Apart from the context of sea level rise, an interesting parameter in ROMS downscaling is SST, which is important in feedback from the ocean to the atmosphere (e.g., Small et al. 2008; Chelton and Xie 2010) and marine ecosystems (e.g., Abdul-Aziz et al. 2011). Figure 16a–c show that the three climate models exhibit the maximal SST increase to the east of the Tsugaru Strait, which suggests that the northward migration of the Kuroshio Current affects these models. The maximal SST warming in ROMS downscaling is reminiscent of the SST change in the climate model (Fig. 16d–f), as downscaling simulations also have maximal SST warming just east of the Tsugaru Strait. However, the magnitude

of the maximal SST warming in ROMS-GFDL is as high as 11 °C, nearly 1.2 times larger than that in the corresponding climate model (9 °C). In addition, ROMS-CSIRO exhibits enhanced SST warming relative to the climate model, whereas maximal SST warming in ROMS-MIROC is only slightly larger than in the climate model. The localized maximal SST change is probably related to the larger northward intrusion of the Kuroshio Current at the end of the twenty-first century than that at the end of the twentieth century in surface current velocities (Figs. 2, 6). The present downscaling model has a bias in the separation latitude of the Kuroshio Current from the eastern coast of Japan. However, the maximal SST increase around the northernmost latitude of the coastal Kuroshio Current in climate models and ROMS downscaling simulations suggests that future changes in the Kuroshio Current may result in large SST change around its separation latitude observed at about 35°N.

4 Summary and discussion

We investigated the future RSL rise in the western North Pacific by conducting dynamical downscaling by using ROMS with eddy-permitting $0.25^\circ \times 0.25^\circ$ resolution. To

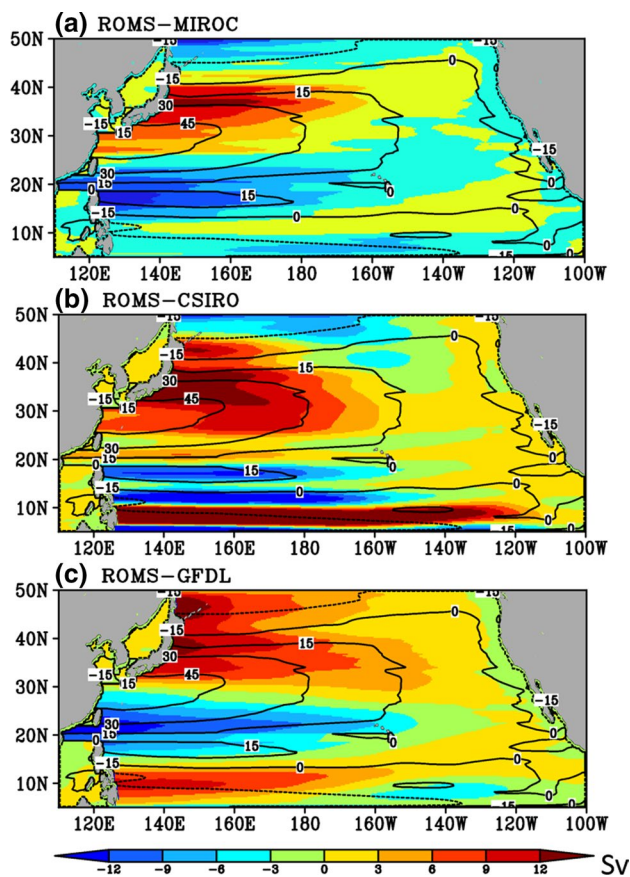


Fig. 14 Projected changes in Sverdrup stream function (Sv, color shading) for 2081–2100 period relative to 1981–2000 period along with their mean value for 1981–2000 (contours) in **a** ROMS-MIROC, **b** ROMS-CSIRO, and **c** ROMS-GFDL. Contour interval is 15 Sv (color figure online)

evaluate the worst cases of RSL rise at the end of twenty-first century around Japan, we selected three climate models that have the highest RSL rise near Japan (Fig. 1), MIROC-ESM, CSIRO-Mk3.6.0, and GFDL-CM3, under the highest greenhouse-gas emission scenario, RCP8.5. Dynamical downscaling was performed for two epochs: the historical run (1950–2000) and the future run (2051–2100). The historical run, ROMS-Hist, is forced by the air-sea fluxes calculated by using COREv2 data. Three future runs—ROMS-MIROC, ROMS-CSIRO, and ROMS-GFDL—are forced with an atmospheric field constructed by adding the difference between the CMIP5 parameters of the twenty-first and twentieth century to the present forcing fields used in ROMS-Hist.

The ROMS downscaling captures finer structures and stronger magnitudes for the RSL changes than those in the CMIP5 models. The downscaled changes commonly exhibit three zonally aligned maxima along 37°N between 140°E and 160°E (Fig. 5). The projected RSL rise maxima during 2081–2100 relative to 1981–2000 reach 63, 67, and 76 cm, in ROMS-MIROC, ROMS-CSIRO, and ROMS-GFDL, respectively (Fig. 5).

All ROMS downscaling commonly shows that the coastal RSL rises are smaller than the offshore RSL rises (Figs. 5, 8), consistent with Sato et al. (2006). The projected RSL rises along the Honshu coast during 2081–2100 relative to 1981–2000 are 19–25, 6–15, and 8–14 cm in ROMS-MIROC, ROMS-CSIRO, and ROMS-GFDL, respectively, which are generally half or less of the RSL rise maxima off the eastern coast of Japan. Moreover, the ranges of RSL changes along the Honshu coast are small in all ROMS downscaling, probably due to shelf waves, which play a role in spatial averaging associated with wave's propagation along the coast (Fig. 9). Although the CMIP5 models underestimate offshore RSL rise maxima substantially than ROMS downscaling (Figs. 5, 7, 8), the discrepancies between the climate models and ROMS downscaling are less than 10 cm along the Honshu coast (Fig. 9). Because the averaging effects of the shelf waves do not contribute to the sea level for islands separated from Honshu, larger RSL changes can occur for some islands than those along Honshu with larger differences between the climate models and ROMS downscaling. At Okinawa Island, the RSL changes are nearly 30 cm in ROMS-MIROC and ROMS-CSIRO, which is higher than the changes along the Honshu coast. The difference in RSL rise at Okinawa Island between ROMS-CSIRO and CSIRO-Mk3.6.0 exceeds 10 cm (Fig. 10).

In ROMS-GFDL, the RSL changes to the east of Japan are accompanied by the zonal velocity changes across KE in the upper 1000 m, penetrating down to 2000 m (Fig. 12), probably due to wind stress changes (e.g., Sakamoto et al. 2005; Sato et al. 2006; Sueyoshi and Yasuda 2012), whereas the shallow velocity and near surface density changes in ROMS-CSIRO suggest that water mass changes play a larger role than the other two models. Both the effects of wind stress and water mass changes are likely to be included in ROMS-MIROC. The RDH changes relative to 2000 dbar reproduce major features of RSL rises very well, including RSL rises associated with the KE changes mainly contributed by the thermosteric component rather than from the halosteric component (Fig. 11).

Other factors that are not taken into account in the present downscaling simulation can influence RSL changes, such as the inverse barometer effect, glacial isostatic adjustment (GIA), gravitational changes resulted from land ice melting and changes of land water storage, and climate model drift (Church et al. 2013; Slangen et al. 2014). The inverse barometer effect, which yields an absolute sea level change less than 3 cm over the North Pacific in all models, is much smaller than the steric and land ice contributions, and hence can be neglected. Based on the IPCC AR5, the GIA and gravitation changes has a relatively small effect around Japan. Climate drifts of the three CMIP5 climate models, which are evaluated using the pre-industry control run, are small for RSL in the western North Pacific, and can be ignored.

In order to obtain information useful for society, it is important to evaluate total sea level rise, which can be

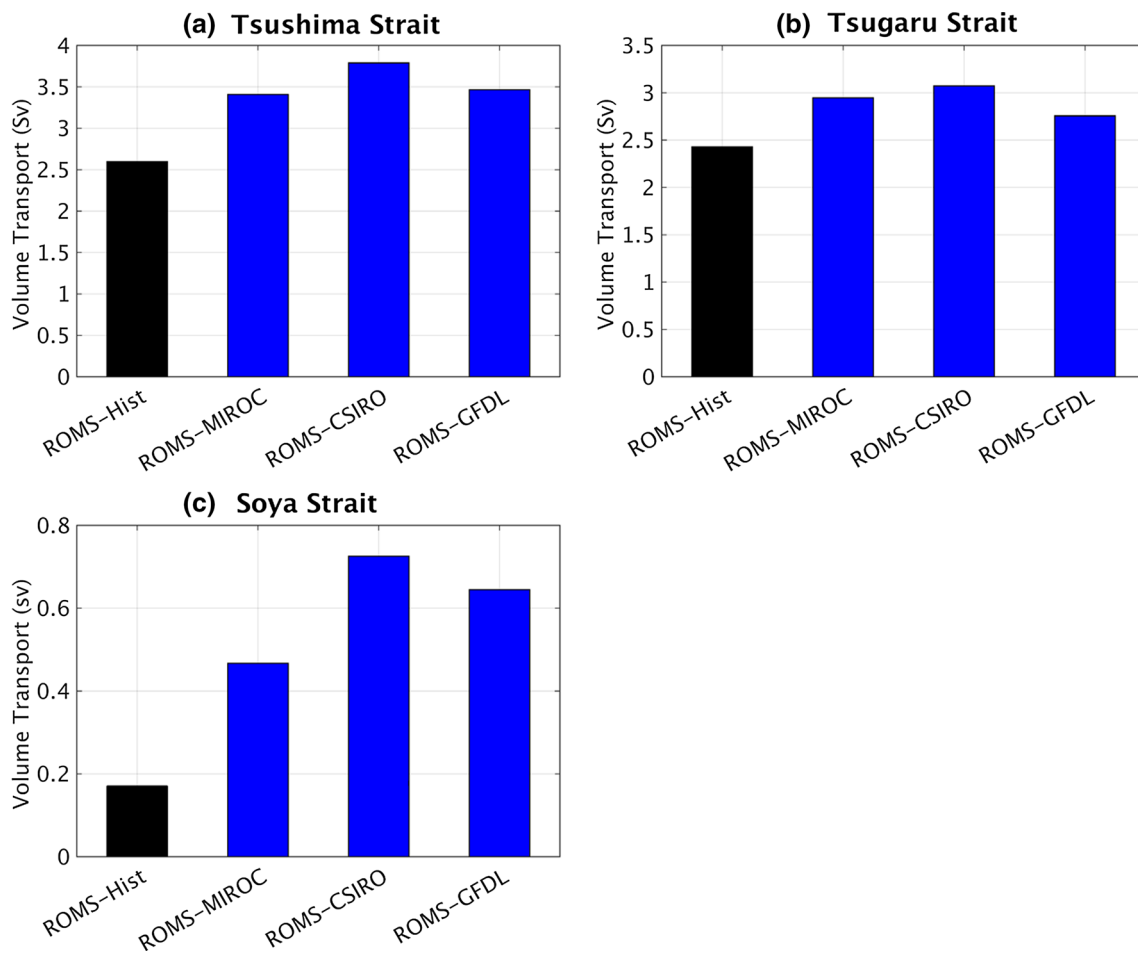


Fig. 15 Time-mean volume transports (in Sv) through **a** Tsushima, **b** Tsugaru, and **c** Soya Strait for 1981–2000 (black) and 2081–2100 (blue) simulated by ROMS downscaling (color figure online)

obtained by the RSL change through downscaling and the global mean sea level rise. Contributions to global mean sea level change include glaciers, land ice and land water storage contributions, thermal expansion contribution, and GIA (Church et al. 2013; Slangen et al. 2014). The GIA effect on the global mean sea level is small (-3 cm in 100 years) (Peltier and Luthcke 2009). The glaciers, land ice, and land water storage contributions to the global mean sea level rise are nearly 16, 16, and 4 cm, respectively, in 2081–2100 relative to 1986–2005 for RCP8.5 in IPCC AR5 (Table 13. SM.1, Church et al. 2013). The thermal expansion components during 2081–2100 relative to 1981–2000 under RCP8.5 are 43, 29, and 36 cm, in MIROC-ESM, CSIRO-Mk3.6.0, and GFDL-CM3, respectively.¹ As a result, the

¹ Globally averaged sea level due to thermal expansion (thermometric component) is estimated with a variable, *zostoga*, in CMIP5. However, *zostoga* is not available for GFDL-CM3, and thus we use another variability, *zossga*, (global average steric sea level change). For MIROC-ESM, both *zostoga* and *zossga* are available and the difference between them are small (less than 0.3 % for 100 year difference).

global mean sea level rise are 79, 65, and 72 cm during 2081–2100 relative to 1981–2000 under RCP8.5 in MIROC-ESM, CSIRO-Mk3.6.0, and GFDL-CM3, as a minor reference period difference of twentieth century, i.e., 1986–2005 in AR5 and 1980–2000 in the present study, can be ignored. Consequently, the coastal sea level rise in total, which is given by the addition of the RSL increase documented in Sect. 3.2 and the global mean sea level rise, are expected to be 101–108, 73–80, and 80–90 cm in MIROC-ESM, CSIRO-Mk3.6.0, and GFDL-CM3, respectively.

An important result in the present study is that the present downscaling reveals that the discrepancy along the Honshu coast between the CMIP5 climate models and corresponding ROMS downscaling is less than 10 cm. Thus, with 10 cm uncertainty, the RSL change along the Honshu coast can be directly evaluated from CMIP5 climate model outputs. This allows the coastal RSL rise to be evaluated with a larger number of climate models (nearly 40), and the probability of sea level changes to be evaluated considering the uncertainties among climate models.

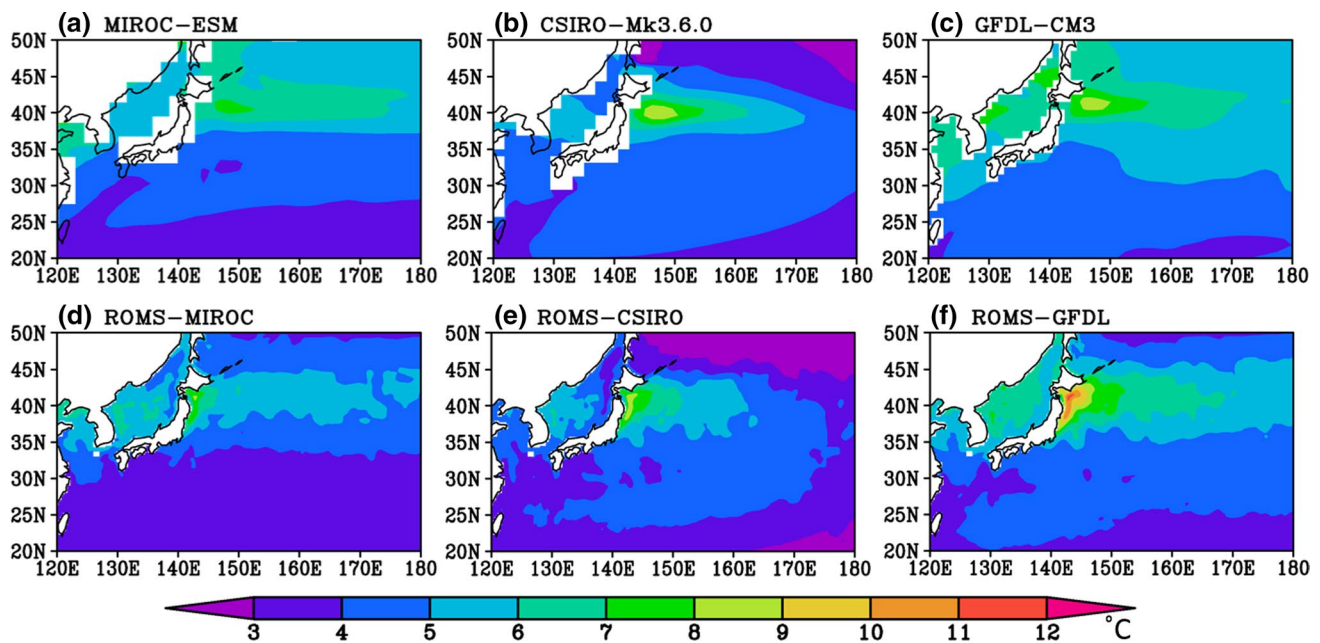


Fig. 16 Projected SST change ($^{\circ}\text{C}$) for 2081–2100 and 1981–2000 in (top) the CMIP5 models and in (bottom) ROMS downscaling simulations for (left) MIROC-ESM, (middle) CSIRO-Mk3.6.0, and (right) GFDL-CM3, respectively

At the eddy-permitting $0.25^{\circ} \times 0.25^{\circ}$ resolution herein, ROMS-Hist exhibits some bias, such as the overshoot of the Kuroshio Current and the northward shift of KE compared with observations. Although we have taken these biases into account in interpreting the downscaled sea level changes, it is not possible to identify the specific locations and magnitudes of the largest coastal sea level rise. To overcome these biases, downscaling with eddy-resolving resolution of $0.1^{\circ} \times 0.1^{\circ}$ may be required. This should be an important research in future, because Tokyo, the most densely city and the capital of Japan, is located near from the separation point of the Kuroshio at 35°N . The computational cost of this resolution is about 16 times larger than that in our experiments, which we expect will become feasible for a number of laboratories in the next decade.

Acknowledgments We are thankful for fruitful discussion with Dr. Tamaki Yasuda and Dr. Tatsuo Suzuki. This work was supported by JSPS KAKENHI Grant Numbers 26287110, 26610146, 15H01606. The numerical calculations were carried out on a computer at the Institute of Low Temperature Science, Hokkaido University.

References

- Abdul-Aziz OI, Mantua NJ, Myers KW (2011) Potential climate change impacts on thermal habitats of Pacific salmon (*Oncorhynchus* spp.) in the North Pacific Ocean and adjacent seas. *Can J Fish Aquat Sci* 68(9):1660–1680. doi:10.113/F2011-079
- Ådlandsvik B (2008) Marine downscaling of a future climate scenario for the North Sea. *Tellus* 60A:451–458. doi:10.1111/j.1600-0870.2008.00311.x
- Antonov JI, Seidov D, Boyer TP, Locarnini RA, Mishonov AV, Garcia HE, Baranova OK, Zweng MM, Johnson DR (2010) World Ocean Atlas 2009. In: Levitus S (ed) Salinity, NOAA Atlas NESDIS 68, vol 2. Government Printing Office, Washington, p 184
- Bindoff NL et al (2007) Observations: Oceanic climate change and sea level. In: Solomon S et al (eds) Climate change 2007: the physical science basis. Contribution of Working Group I to the Fourth Assessment Report of the Intergovernmental Panel on Climate Change. Cambridge University Press, Cambridge
- Carton JA, Giese BS (2008) A reanalysis of ocean climate using Simple Ocean Data Assimilation (SODA). *Mon Weather Rev* 136(8):2999–3017
- Cazenave A, Cozannet GL (2013) Sea level rise and its coastal impacts. *Earths Future* 2:15–34. doi:10.1002/2013EF000188
- Chamberlain MA, Sun CJ, Matear RJ, Feng M, Phipps SJ (2012) Downscaling the climate change for oceans around Australia. *Geosci Model Dev* 5:1177–1194
- Chelton DB, Xie SP (2010) Coupled ocean-atmosphere interaction at oceanic mesoscales. *Oceanography* 23(4):52–69
- Church JA et al (2013) Sea Level Change. In: Stocker TF et al (eds) Climate change 2013: the physical science basis. Contribution of Working Group I to the Fifth Assessment Report of the Intergovernmental Panel on Climate Change. Cambridge University Press, Cambridge
- Curchitser EN, Haidvogel DB, Hermann AJ, Dobbins EL, Powell TM, Kaplan A (2005) Multi-scale modeling of the North Pacific Ocean: assessment and analysis of simulated basin-scale variability (1996–2003). *J Geophys Res*. doi:10.1029/2005JC002902
- Ducet N, Le Traon PY, Reverdin G (2000) Global high resolution mapping of ocean circulation from TOPEX/Poseidon and ERS-1/2. *J Geophys Res* 105(19):477–498

- Fairall CW, Bradley EF, Hare JE, Grachev AA, Edson JB (2003) Bulk parameterization of air-sea fluxes: updates and verification for the COARE algorithm. *J Clim* 16:571–591
- Fukamachi Y, Ohshima KI, Ebuchi N, Bando T, Ono K, Sano M (2010) Volume transport in the Soya strait during 2006–2008. *J Oceanogr* 66:685–696
- Fukudome K, Yoon JH, Ostrovskii A, Takikawa T, Han IS (2010) Seasonal volume transport variation in the Tsushima warm current through the Tsushima Straits from 10 years of ADCP observations. *J Oceanogr* 66:539–551
- Gill AE (1982) *Atmosphere-ocean dynamics*. Academic Press, Harcourt Place, London, p 215
- Griffies SM et al (2005) Formulation of an ocean model for global climate simulations. *Ocean Sci* 1:45–79
- Griffies SM, Winton M, Donner LJ et al (2011) The GFDL CM3 coupled climate model: characteristics of the ocean and sea ice simulations. *J Clim* 24:3520–3544. doi:10.1175/2011JCLI3964.1
- Haidvogel DB, Arango HG, Hedstrom K, Beckmann A, Malanotte-Rizzoli P, Shchepetkin AF (2000) Model evaluation experiments in the North Atlantic basin: simulations in nonlinear terrain-following coordinates. *Dyn Atmos Oceans* 32:239–281
- Han W, Moore AM, Levin J, Zhang B, Arango HG, Curchitser E, Lorenzo ED, Gordon AL, Lin J (2009) Seasonal surface ocean circulation and dynamics in the Philippine Archipelago region during 2004–2008. *Dyn Atmos Oceans* 47:114–137
- Hanson S, Nicholls R, Ranger N, Hallegatte S, Corfee-Morlot J, Herweijer C, Chateau J (2011) A global ranking of port cities with high exposure to climate extremes. *Clim Change* 104:89–111. doi:10.1007/s10584-010-9977-4
- Ito T, Togawa O, Ohnishi M, Isoda Y, Nakayama T, Shima S, Kuroda H, Iwahashi M, Sato C (2003) Variation of velocity and volume transport of the Tsugaru warm current in the winter of 1999–2000. *Geophys Res Lett* 30(13):1678. doi:10.1029/2003GL017522
- Jeffrey SJ, Rotstayn L, Collier M, Dravitzk S, Hamalaien C, Moeseneder C, Wong K, Syktus J (2013) Australia's CMIP5 submission using the CSIRO Mk3.6 model. *Aust Meteorol Oceanogr J* 63:1–13
- Kagimoto T, Yamagata T (1997) Seasonal transport variations of the Kuroshio: an OGCM simulation. *J Phys Oceanogr* 27:403–418
- Landerer FW, Jungclaus JH, Marotzke J (2007) Regional dynamic and steric sea level change in response to the IPCC = A1B scenario. *J Phys Oceanogr* 37:296–312
- Large WG, Yeager S (2009) The global climatology of an interannually varying air-sea flux data set. *Clim Dyn* 33:341–364. doi:10.1007/s00382-008-0441-3
- Large WG, McWilliams JC, Doney SC (1994) Oceanic vertical mixing: a review and a model with a nonlocal boundary layer parameterization. *Rev Geophys* 32:363–404
- Lee T, Waliser DE, Li JF, Landerer FW, Gierach MM (2013) Evaluation of CMIP3 and CMIP5 wind stress climatology using satellite measurements and atmospheric reanalysis products. *J Clim* 26:5810–5826. doi:10.1175/JCLI-D-12-00591.1
- Liu Z, Wu L (1999) Rossby wave-coastal kelvin wave interaction in the extratropics. Part II: formation of island circulation. *J Phys Oceanogr* 29:2405–2418
- Liu Y, Xie L, Morrison JM, Kamykowski D (2013) Dynamic downscaling of the impact of climate change on the ocean circulation in the Galápagos Archipelago. *Adv Meteorol* 2013:1–18
- Liu Y, Lee SK, Enfield DB, Muhling BA, Lamkin JT, Muller-Karger FE, Roffer MA (2015) Potential impact of climate change on the Intra-Americas Sea: Part-1. A dynamic downscaling of the CMIP5 model projections. *J Mar Sys* 148(2015):56–69
- Locarnini RA, Mishonov AV, Antonov JI, Boyer TP, Garcia HE, Baranova OK, Zweng MM, Johnson DR (2010) *World Ocean Atlas 2009*. In: Levitus S (ed) *Temperature*, NOAA Atlas NESDIS 68, vol 1. Government Printing Office, Washington, p 184
- Lorenzo ED, Schneider N, Cobb KM, Franks PJS, Chhak K et al (2008) North Pacific gyre oscillation links ocean climate and ecosystem change. *Geophys Res Lett* 35(L08607):1–6. doi:10.1029/2007GL032838
- Lowe JA, Gregory M (2006) Understanding projections of sea level rise in a Hadley Centre coupled climate model. *J Geophys Res*. doi:10.1029/2005JC003421
- Lyu SJ, Kim K (2005) Subinertial to interannual transport variations in the Korea Strait and their possible mechanisms. *J Geophys Res* 110(C1206). doi:10.1029/2004JC002651
- Marchesiello P, McWilliams JC, Shchepetkin A (2001) Open boundary conditions for long-term integration of regional oceanic model. *Ocean Model* 3:1–20
- Meier HEM (2006) Baltic Sea climate in the late twenty-first century: a dynamical downscaling approach using two global models and two emission scenarios. *Clim Dyn* 27(1):39–68. doi:10.1007/s00382-006-0124-x
- Moss RH, Edmonds JA, Hibbard KA et al (2010) The next generation of scenarios for climate change research and assessment. *Nature* 463:747–756. doi:10.1038/nature08823
- Nicholls RJ, Hanson S, Herweijer C, Patmore N, Hallegatte S et al (2008) Ranking port cities with high exposure and vulnerability to climate extremes: exposure estimates. *OECD Publ*. doi:10.1787/011766488208
- Ohshima KI (1994) The flow system in the Japan Sea caused by a sea level difference through shallow straits. *J Geophys Res* 99:9925–9940
- Oliver ECJ, Holbrook NJ (2014) Extending our understanding of South Pacific gyre “spin-up”: modeling the East Australian current in a future climate. *J Geophys Res Ocean* 119:2788–2805. doi:10.1002/2013JC009591
- Peltier WR, Luthcke SB (2009) On the origins of Earth rotation anomalies: new insights on the basis of both “paleogeodetic” data and gravity recovery and climate experiment (GRACE) data. *J Geophys Res*. doi:10.1029/2009JB006352
- Rio MH, Hernandez F (2004) A mean dynamic topography computed over the world ocean from altimetry, in situ measurements, and a geoid model. *J Geophys Res*. doi:10.1029/2003JC002226
- Rotstayn LD et al (2010) Improved simulation of Australian climate and ENSO-related rainfall variability in a global climate model with an interactive aerosol treatment. *Int J Climatol* 30:1067–1088. doi:10.1002/joc.1952
- Sakamoto TT, Hasumi H, Ishii M, Emori S, Suzuki T, Nishimura T, Sumi A (2005) Responses of the Kuroshio and the Kuroshio extension to global warming in a high-resolution climate model. *Geophys Res Lett*. doi:10.1029/2005GL023384
- Sasaki YN, Minobe S, Miura Y (2014) Decadal sea-level variability along the coast of Japan in response to ocean circulation changes. *J Geophys Res Oceans* 119:266–275. doi:10.1002/2013JC009327
- Sato Y, Yukimoto S, Tsujino H, Ishizaki H, Noda A (2006) Response of North Pacific ocean circulation in a Kuroshio-resolving ocean model to an Arctic Oscillation (AO)-like change in Northern Hemisphere atmospheric circulation due to greenhouse-gas forcing. *J Meteorol Soc Jpn* 84:295–309
- Seo H, Miller AJ, Roads JO (2007) The scripps coupled ocean-atmosphere regional (SCOAR) model, with applications in the eastern Pacific sector. *J Clim* 20:381–402
- Seo GH, Cho YK, Choi BJ, Kim KY, Kim BG, Tak YJ (2014) Climate change projection in the Northwest Pacific marginal seas through dynamic downscaling. *J Geophys Res Oceans* 119:3497–3516. doi:10.1002/2013JC009646
- Shchepetkin AF, McWilliams JC (2005) The regional oceanic modeling system (ROMS): a split-explicit, free-surface,

- topography-following-coordinate ocean model. *Ocean Model* 9:347–404
- Shu Q, Qian FL, Song ZY, Yin XQ (2013) A comparison of two global ocean-ice coupled models with different horizontal resolutions. *Acta Oceanol Sin* 32(8):1–11
- Slangen ABA, Carson M, Katsman CA et al (2014) Projecting twenty-first century regional sea-level changes. *Clim Change* 124:317–332
- Small RJ, deSzoeko SP, Xie SP, O'Neill L, Seo H, Song Q, Cornillon P, Spall M, Minobe S (2008) Air-sea interaction over ocean fronts and eddies. *Dyn Atmos Oceans* 45:274–319. doi:[10.1016/j.dynatmoce.2008.01.001](https://doi.org/10.1016/j.dynatmoce.2008.01.001)
- Sueyoshi M, Yasuda T (2012) Inter-model variability of projected sea level changes in the western North Pacific in CMIP3 coupled climate models. *J Oceanogr* 68:533–543. doi:[10.1007/s10872-012-0117-9](https://doi.org/10.1007/s10872-012-0117-9)
- Sumata H, Hashioka T, Suzuki T, Yoshie N, Okunishi T, Aita MN, Sakamoto TT, Ishida A, Okada N, Yamanaka Y (2010) Effect of eddy transport on the nutrient supply into the euphotic zone simulated in an eddy-permitting ocean ecosystem model. *J Mar Sys* 83(2010):67–87. doi:[10.1016/j.jmarsys.2010.07.002](https://doi.org/10.1016/j.jmarsys.2010.07.002)
- Sun CJ, Feng M, Matear RJ, Chamberlain MA, Craig P, Ridgway KR, Schiller A (2012) Marine downscaling of a future climate scenario for Australian boundary currents. *J Clim* 25(8):2947–2962. doi:[10.1175/JCLI-D-11-00159.1](https://doi.org/10.1175/JCLI-D-11-00159.1)
- Suzuki T, Ishii M (2011a) Regional distribution of sea level changes resulting from enhanced greenhouse warming in the Model for Interdisciplinary Research on Climate version 3.2. *Geophys Res Lett*. doi:[10.1029/2010GL045693](https://doi.org/10.1029/2010GL045693)
- Suzuki T, Ishii M (2011b) Long-term regional sea level changes due to variations in water mass density during the period 1981–2007. *Geophys Res Lett*. doi:[10.1029/2011GL049326](https://doi.org/10.1029/2011GL049326)
- Tokeshi T, Yanagi T (2003) High sea level caused at Naha in Okinawa Island. *Oceanogr Jpn* 12(4):395–405 (**in Japanese with English abstract**)
- Tsujino H, Nakano H, Motoi T (2008) Mechanism of currents through the straits of the Japan Sea: mean state and seasonal variation. *J Oceanogr* 64:141–161
- Watanabe S, Hajima T, Sudo K et al (2011) MIROC-ESM 2010: model description and basic results of CMIP5-20c3m experiments. *Geosci Model Dev* 4:845–872. doi:[10.5194/gmd-4-845-2011](https://doi.org/10.5194/gmd-4-845-2011)
- Yin J (2012) Century to multi-century sea level rise projections from CMIP5 models. *Geophys Res Lett*. doi:[10.1029/2012GL052947](https://doi.org/10.1029/2012GL052947)
- Yin J, Griffies SM, Stouffer RJ (2010) Spatial variability of sea level rise in twenty-first century projections. *J Clim* 23:4585–4607. doi:[10.1175/2010JCLI3533.1](https://doi.org/10.1175/2010JCLI3533.1)
- Zhang XB, Church JA, Platten SM, Monselesan D (2014) Projection of subtropical gyre circulation and associated sea level changes in the Pacific based on CMIP3 climate models. *Clim Dyn* 43:131–144. doi:[10.1007/s00382-013-1902-x](https://doi.org/10.1007/s00382-013-1902-x)